

CENTRAL ASIAN JOURNAL OF THEORETICAL AND APPLIED SCIENCE

https://cajotas.casjournal.org/index.php/cajotas

Volume: 07 Issue: 04 | October 2026 ISSN: 2660-5317

Article

Synthesis, Spectroscopic, Nano-Structure, Biological Activity Study of Zirconium (IV) Complexes with Thione Ligands

Anwar Adel Hameed[1]

1. Department of Chemistry, College of Science, University of Tikrit

* Correspondence: Anwar.adel@tu.edu.iq

Abstract: Three new zirconium(IV) complexes with thione ligands 2-mercaptobenzothiazole (MBT), 2-mercaptobenzimidazole (MBI) and 1-methyl-1H-tetrazole-5-thiol (HMtzS) have been synthesized and characterized by FT-IR, 1H NMR, molar conductance, PXRD, SEM and EDX analysis. The analytical data were consistent with the formation of complexes of general formula [ZrO(thione)2], where each thione ligand coordinates to the Zr(IV) ion in a bidentate (S,N) fashion through the deprotonated thiolate sulfur and the heterocyclic ring nitrogen atom. The molar conductance measurements showed that all complexes are non-electrolytes. PXRD analysis showed that [ZrO(MBT)2] has a relatively well-defined crystalline structure with an average crystalline size of ~35.7 nm, while [ZrO(MBI)2] and [ZrO(MtzS)2] were predominantly amorphous or poorly crystalline. SEM images revealed different morphologies, [ZrO(MBT)2] exhibited a dense layered fibrous structure whereas [ZrO(MBI)2] and [ZrO(MtzS)2] presented a highly agglomerated cauliflower-like granular morphology with particle sizes in the range of 38-230 nm. EDX analysis confirmed the presence of Zr, S, C, O and N in the complexes. Antibacterial activity of free ligands and their Zr(IV) complexes were evaluated against Staphylococcus aureus, Staphylococcus epidermidis and Escherichia coli. All the complexes exhibited higher antibacterial activity than their corresponding free ligands and $[ZrO(MBI)_2]$ possessed the most balanced and potent activity against all three strains (19, 17 and 18 mm, respectively) while $[ZrO(MtzS)_2]$ showed the highest activity against S. epidermidis (21 mm). The complexes were not superior than the standard antibiotic tetracycline but comparable to it which indicates their potential as promising antibacterial agents.

Keywords: zirconium, thione, benzothiazole, SEM, XRD, biological activity

Citation: Hameed, A. A. Synthesis, Spectroscopic, Nano-Structure, Biological Activity Study of Zirconium (IV) Complexes with Thione Ligands. Central Asian Journal of Theoretical and Applied Science 2026, 7(4), 249-262

Received: 13th Jul 2026
Revised: 28th Aug 2026
Accepted: 15th Sep 2026
Published: 10th Oct 2026

Copyright: © 2026 by the authors. Submitted for open access publication under the terms and conditions of the Creative Commons Attribution (CC BY) license (https://creativecommons.org/licenses/by/4.0/)

1. Introduction

The coordination chemistry of zirconium (IV) has been a topic of sustained interest for several decades, primarily due to the unique electronic configuration of the Zr^{4+} ion (d^0), its high charge-to-radius ratio and its pronounced oxophilicity, which in combination lead to the formation of complexes with high coordination numbers and diverse stereochemistry's [1], [2], [3], [4]. Among the various classes of ligands which have attracted much attention in zirconium coordination chemistry are sulfur donor ligands, particularly thiones [5], [6], [7], [8], [9], [10], [11]. Thione ligands are characterized by the presence of an exocyclic double bond between carbon and sulfur (C=S) within a heterocyclic or acyclic framework. These ligands possess a combination of strong sigma-donation from sulfur and the capacity for pi-back-bonding interactions, which makes them versatile chelating agents for early transition metals in high oxidation states [12], [13], [14], [15], [16], [17], [18], [19], [20], [21], [22], [23], [24], [25], [26], [27], [28], [29], [30], [31]. The zirconium-thione complexes obtained are of interest not only due to their basic

structural and electronic properties, but also for their potential application in biological and catalytic areas [30], [31], [32], [33], [34], [35], [36], [37].

Thione ligands are important in coordination chemistry mainly because they can exist in tautomeric equilibrium with the corresponding thiol (S-H) forms, which influences significantly their coordination behavior. In the thione tautomer, coordination typically occurs through the sulfur atom while the N–H proton remains intact; in the thiol form, deprotonation may accompany metal binding, leading to thiolate complexes [5], [6], [7], [8], [9], [10], [11]. This tautomeric flexibility, coupled with the presence of additional donor atoms such as nitrogen or oxygen within the ligand framework, enables thiones to act as monodentate, bidentate, or even polydentate ligands. For zirconium (IV), which exhibits a strong preference for hard donor atoms, the interplay between hard nitrogen/oxygen donors and the softer sulfur donor creates interesting possibilities for mixed-donor coordination spheres and for fine-tuning of the metal's electronic environment [35], [38], [39], [40], [41]. This work aims to synthesize, spectroscopically characterize, and evaluate the nano-structural features and biological activity of zirconium (IV) complexes with selected thione ligands. The study employs a combination of established spectroscopic techniques (FT-IR, ^{1}H and ^{13}C NMR), molar conductance and magnetic measurements, and complementary methods for nano-structural analysis. Biological evaluation includes antimicrobial assays to establish preliminary structure–activity relationships. The results are expected to deepen understanding of zirconium–thione coordination chemistry.

2. Materials and Methods

2.1 Materials and instrumentation

The chemicals material included hydrated zirconium oxychloride ($ZrOCl_2{\cdot}8H_2O$), the ligands 2-mercaptobenzothiazole (MBT), 2-mercaptobenzimidazole (2-MBI) and 1-methyl-1H-tetrazole-5-thiol (H-MtzS), sodium hydroxide (NaOH), and absolute ethanol as solvent were used as received without further purification.

2.2 Synthesis of the metal complexes

2.2.1 Synthesis of $[ZrO(MBT)_2]$(1)

In a 100 mL round-bottomed flask, a hot ethanolic solution of 2-mercaptobenzothiazole (MBT) (0.311 g, 1.859 mmol) was treated with sodium hydroxide (NaOH) (0.080 g, 2.000 mmol) and the resulting mixture was added dropwise, with continuous stirring, to a hot ethanolic solution of hydrated zirconium oxychloride, $ZrOCl_2{\cdot}8H_2O$ (0.300 g, 0.939mmol). The mixture was refluxed for 3 h then a yellowish-white precipitate formed after approximately 30 min form the begin of reflux. The precipitate was filtered off, washed with absolute ethanol, and dried to give a yellowish-white ppt.

2.2.2 Synthesis of $[ZrO(2\text{-}MBI)_2]$ (2)

In a 100 mL round-bottomed flask, a hot ethanolic solution of 2-mercaptobenzimidazole (2-MBI) (0.27 g, 1.79 mmol) was treated with sodium hydroxide (NaOH) (0.070 g, 1.75 mmol) and the mixture was added to a hot ethanolic solution of hydrated zirconium oxychloride (0.3 g, 0.930 mmol)with continuous stirring, and the mixture was refluxed for 3 h. then a white precipitate formed after approximately 30 min. form the begin of reflux. The precipitate was filtered off, washed with ethanol, and dried to give a white ppt.

2.2.3 Synthesis of $[ZrO(H\text{-}MtzS)_2]$ (3)

In a 100 mL round-bottomed flask, a hot ethanolic solution of 1-methyl-1H-tetrazole-5-thiol (H-MtzS) (0.14 g, 1.2 mmol) was treated with sodium hydroxide (NaOH) (0.04 g, 1 mmol) and the mixture was added to a hot ethanolic solution of hydrated zirconium oxychloride (0.2 g, 0.62 mmol) with continuous stirring, and the mixture was refluxed for 3 h. a white precipitate formed after approximately 15 min. form the begin of reflux. The precipitate was filtered off, washed with ethanol, and dried to give a white ppt.

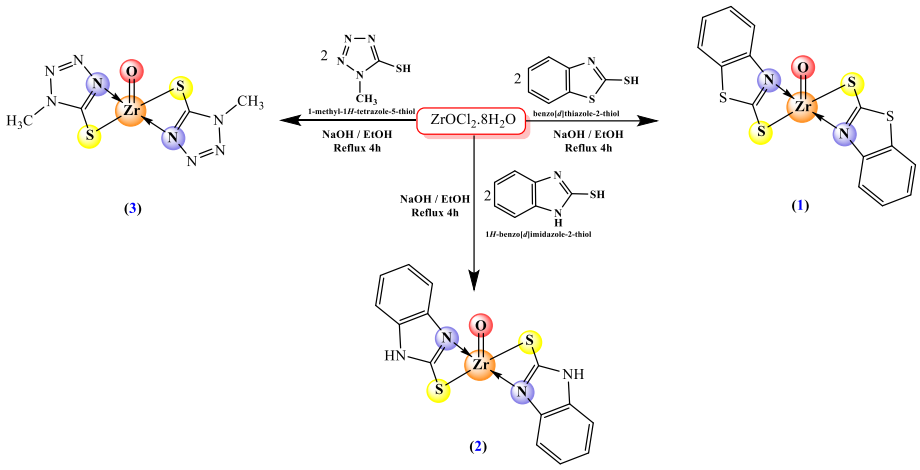
2.3 antibacterial study

The antibacterial effectiveness of the unbound ligand and its newly formed complexes was evaluated using the agar diffusion method against four harmful bacteria: *Staphylococcus epidermidis, Staphylococcus aureus, and Escherichia coli*. The microorganisms

were grown in LB Broth at 37 ˚C with stirring at 130 revolutions per minute in an incubator. On firm nutritional agar plates, 100 microliters of culture broth with 10^6 colony-forming units per milliliter of each test organism was applied to establish a bacterial culture lawn. A period of ten to fifteen minutes was allocated for the plates to stay undisturbed, allowing the culture to assimilate their contents. Wells measuring 8 millimeters in diameter were formed in the agar using sterile micropipette tips. Utilizing a micropipette, the chemical solution prepared in DMSO (10^{-3} M) was allocated into the wells of each plate. The measurements of the inhibitory zone were evaluated at 37 ˚C after a 24-hour incubation. The tetracycline antibiotic solution served as the positive control in this research.

3. Results

Treatment two equivalent mole of the thione ligand {benzo[d]thiazole-2-thiol (HMBT), 1H-benzo[d]imidazole-2-thiol (HMBI), 1-methyl-1H-tetrazole-5-thiol (HMtzS)} with the one equivalent mole of $ZrOCl_2$ salt in basic medium afforded complexes of the type [ZrO(thione)$_2$] where (thione = MBT^-, MBI^-, and $MtzS^-$ } as a solo product (Scheme 1).



Scheme 1: synthetic pathway of the prepared complexes

The design of the newly synthesized compounds was ascertained by various techniques, including infrared spectroscopy (FT-IR), proton nuclear magnetic resonance (^{1}H NMR), and molar conductivity, whereas the nanostructures were analyzed using XRD and SEM. The physical and characteristic data is presented in **Table 1**.

Table 1. Physical properties of the synthesized complexes.

Seq	Complexes	Color	m.p. (°C)	Λm (S·cm²·mol⁻¹)	Yield (%)
1	[ZrO(MBT)$_2$]	Yellowish-white	277–280	1.40	50
2	[ZrO(MBI)$_2$]	White	> 300 not melts	3.85	90
3	[ZrO(MtzS)$_2$]	White	320	1.71	65

.

Molar conductance (Λm) was measured for 10^{-3} M solutions in DMSO solution at room temperature, the low values obtained for all three complexes indicate their non-electrolytic nature.

3.1 IR data

The spectrum of the free ligand (MBT) displayed four characteristic absorption bands at (3042–2963) cm^{-1}, 1595 cm^{-1}, 1319 cm^{-1} and 1246 cm^{-1}, assigned respectively to the aromatic and aliphatic ν(C–H) stretching vibrations, ν(C=N), ν(C–N) and ν(C–S). The ν(S–H) band characteristic of the free ligand at 2667 cm^{-1} disappeared in the spectrum of the

complex, supporting deprotonation of the thiol group and its conversion to the anionic (thiolate) form, coordinated to the metal ion through the thiol sulfur atom. The ν(C=N) band shifted to a higher frequency, appearing at 1624 cm^{-1} in the complex, indicating participation of the heterocyclic ring nitrogen atom in coordination to the metal ion. Finally, two new low-frequency bands appeared in the spectrum of the complex at 601 and 476 cm^{-1}, assigned to ν(Zr–S) and ν(Zr–N), respectively, confirming bidentate (S,N) coordination of the ligand to the metal ion. While, the spectrum of the free ligand (2-MBI) showed characteristic bands at 3047 cm^{-1}, 1624 cm^{-1} and 1359 cm^{-1}, assigned to aromatic ν(C–H), ν(C=N) and ν(C–N), respectively. The ν(S–H) band at 2571 cm^{-1} disappeared in the spectrum of the complex, supporting deprotonation of the thiol group and coordination through the sulfur atom. The ν(C=N) band shifted from 1624 cm^{-1} in the free ligand to 1591 cm^{-1} in the complex — a shift to lower frequency indicating coordination of the heterocyclic ring nitrogen atom to the metal ion. Two new low-frequency bands appeared at 538 and 451 cm^{-1}, assigned to ν(Zr–S) and ν(Zr–N), respectively. Whereas the spectrum of the free ligand (HMtzS) showed characteristic bands at 2974 cm^{-1}, 1510 cm^{-1}, 1354 cm^{-1} and 1163 cm^{-1}, assigned to ν(C–H), ν(C=N), ν(N=N) and ν(N–N), respectively. The ν(S–H) band at 2737 cm^{-1} disappeared in the spectrum of the complex, supporting deprotonation of the thiol group and coordination through the sulfur atom. The ν(C=N) band shifted from 1510 cm^{-1} in the free ligand to 1582 cm^{-1} in the complex, indicating coordination of the heterocyclic ring nitrogen atom to the metal ion. Two new low-frequency bands appeared at 518 and 439 cm^{-1}, assigned to ν(Zr–S) and ν(Zr–N), respectively. Taken together, these results confirm that all three ligands coordinate to the Zr(IV) ion in a bidentate (S,N) fashion, through the deprotonated (thiolate) sulfur atom and the heterocyclic ring nitrogen atom.

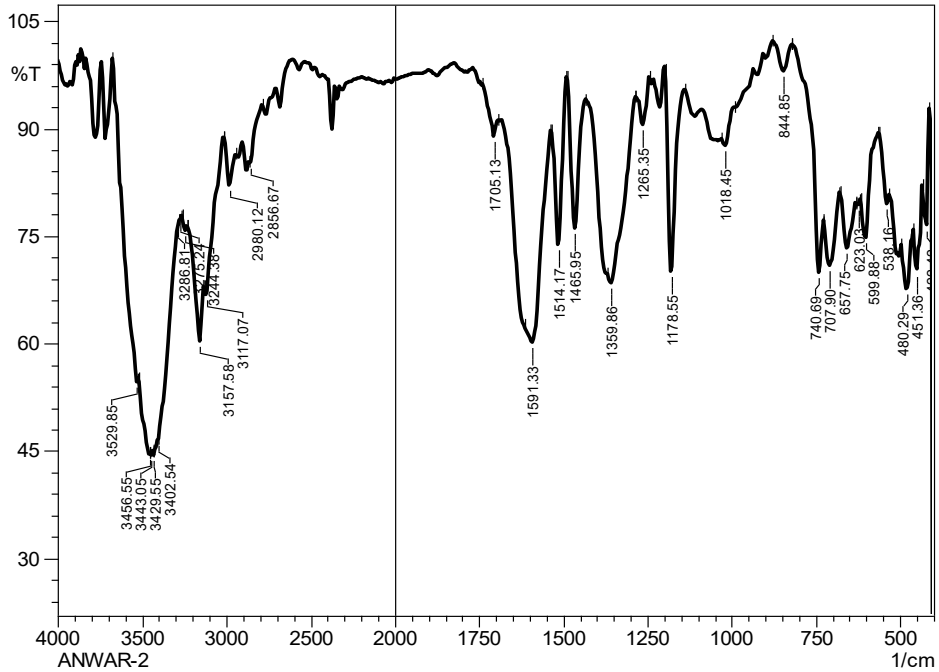


Figure 1. IR spectrum of the $[ZrO(MBT)_2]$ complex

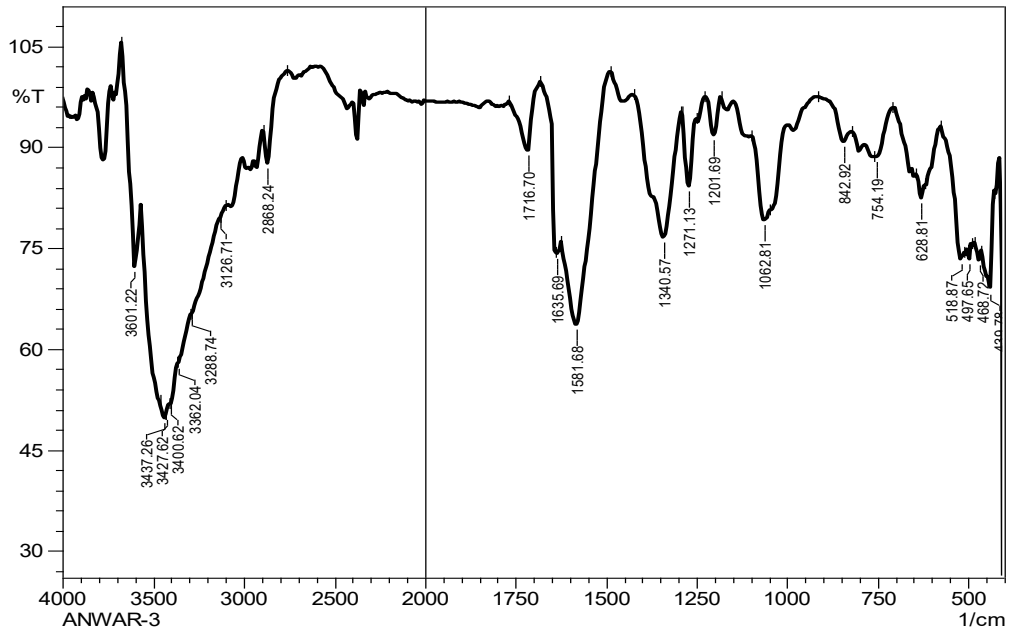


Figure 2. IR spectrum of the [ZrO(MBI)$_2$] complex

3.2 NMR data

The ^{1}H NMR spectrum of the [ZrO(MBT)$_2$] complex (**1**) (**Figure 3**) clearly showed the disappearance of the proton of the S–H group (which displayed at 13.46 ppm in free ligand), facilitating the deprotonation of the thiol group and its transformation into the anionic (thiolate) state, bound to the metal ion via the sulfur atom of the thiol group. Also, spectrum of the complex displayed the protons of the aromatic ring as two peaks, first peak showed as multiplet peak at δH = 7.35 ppm due to the protons in **3**-**4** positions, and the second peak displayed as a doublet of doublets at δH = 7.70 ppm (2H, *J* 8.30, 1.89 Hz) due to the proton in position **1**. In similar the ^{1}H NMR spectrum of the [ZrO(MBI)$_2$] complex (**2**) clearly showed the disappearance of the proton of the S–H group (which displayed at 12.78 ppm in free ligand), facilitating the deprotonation of the thiol group and its transformation into the anionic (thiolate) state, bound to the metal ion via the sulfur atom of the thiol group. Also, spectrum of the complex displayed the protons of the aromatic ring as two multiplet peaks, first peak at δH = 7.27 ppm due to the protons in **2** and **3** positions, and the second peak at δH = 7.68 ppm due to the proton in position **1** and **4**. The ^{1}H NMR spectrum of the [ZrO(MtzS)$_2$] complex (**3**) (**Figure 4**) clearly showed the disappearance of the proton of the S–H group (which displayed at 13.21 ppm in free ligand), supporting the deprotonation of the thiol group and its transformation into the anionic (thiolate) state. Also, spectrum of the complex displayed the protons of the methyl group singlet peak at δH = 2.41 ppm.

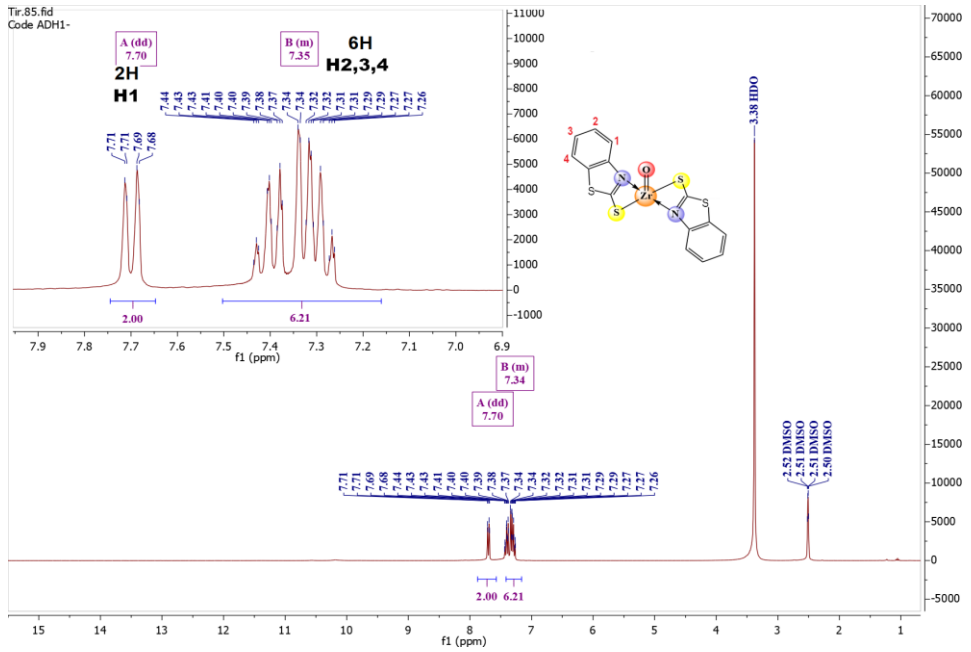


Figure 3. ^{1}H NMR spectrum of the [ZrO(MBT)$_2$] complex

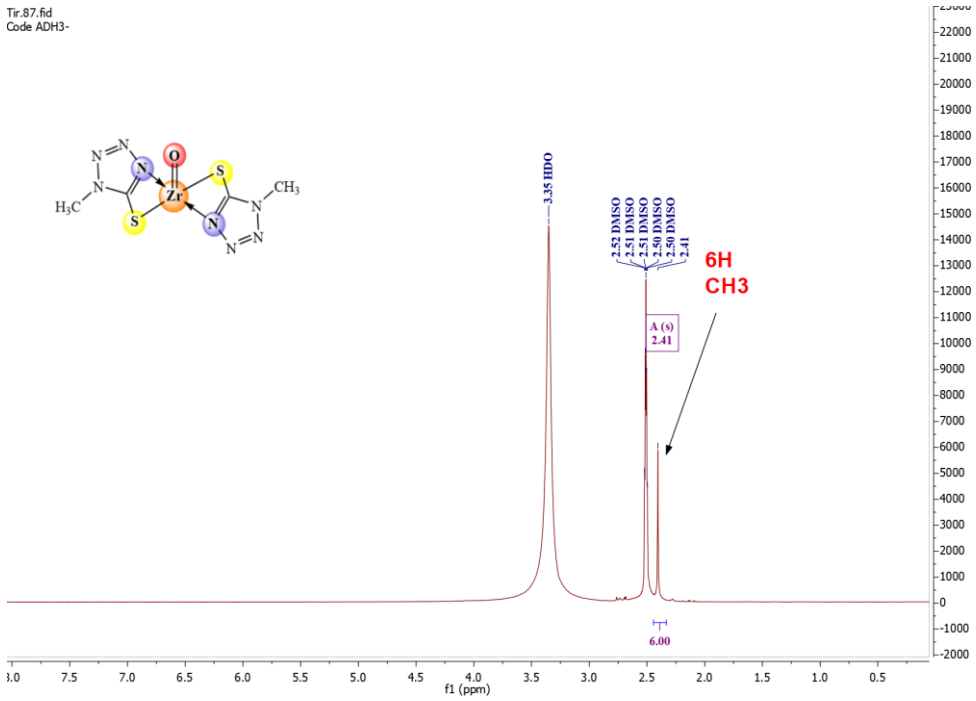


Figure 4. ^{1}H NMR spectrum of the [ZrO(MtzS)$_2$] complex

3.3 Powder X-ray diffraction (PXRD) analysis

Powder X-ray diffraction (PXRD) was used to characterize the crystalline nature of the prepared complexes. This technique provides accurate structural data for well-crystallized materials, whereas for poorly crystalline powders the derived parameters are less precise, although they still provide useful qualitative information on the degree of structural order. In a PXRD pattern, the diffracted intensity is plotted as a function of the scattering angle (2θ); constructive interference occurs at angles satisfying Bragg's law, producing a well-defined diffraction peak, whereas deviation from the Bragg condition results in destructive interference and no observable peak [**42**].

Bragg's law can be expressed in the form:

$$(\lambda / 2a)^2 = sin^2\theta / (h^2 + k^2 + l^2) \quad \text{---------- (1)}$$

where λ is the wavelength of the X-ray radiation used, a is the unit-cell parameter, θ is the Bragg angle, and h, k, l are the Miller indices. Since λ and a are constant for a given sample, the term $(\lambda/2a)^2$ is constant, and hence the ratio $\sin^2\theta/(h^2+k^2+l^2)$ is also constant; the denominator $(h^2+k^2+l^2)$ therefore varies with θ in a manner that preserves this ratio. Applying this relationship allowed the Miller indices corresponding to each observed Bragg angle to be assigned [42], [43]. This indexing was carried out only for $[ZrO(MBT)_2]$ complex, which displayed sharp, high-intensity peaks, whereas indexing of complexes $[ZrO(MBI)_2]$ and $[ZrO(MtzS)_2]$ was not possible owing to the absence of a sufficient number of well-resolved sharp peaks, as shown in **Table 3**.

PXRD patterns of the three complexes were also used to estimate the average crystallite size using the Debye–Scherrer equation, which relates the crystallite size to the full width at half maximum (FWHM) of a diffraction peak according to:

$$D = (K \times \lambda) / (\beta \cos\theta) \quad \text{----------(2)}$$

where D is the crystallite size, λ is the X-ray wavelength, K is a dimensionless shape constant (commonly taken as 0.9), β is the FWHM of the peak in radians, and θ is the Bragg angle [42], [43]. Using Cu-Kα radiation (λ = 1.5406 Å = 0.15406 nm), Equation (3) reduces to:

$$D = (0.9 \times 0.15406) / (\beta \cos\theta) = 0.13865 / (\beta \cos\theta) \quad \text{----------(3)}$$

The diffraction pattern of complex $[ZrO(MBT)_2]$ exhibited a number of relatively sharp, well-defined Bragg reflections, particularly within the range $2\theta \approx 23–29°$, indicating a higher degree of long-range crystalline order compared with the other two complexes, as shown in **Figure 5**. Ten resolved peaks were analyzed in this pattern, giving apparent D values ranging from approximately 23.22 to 49.16 nm, with a mean value of about 35.70 nm (**Table 3**). These values represent apparent sizes of the coherently diffracting domains rather than direct particle diameters, since peak broadening may also include contributions from instrumental broadening and macrostrain within the crystal lattice. Overall, the sharp and intense diffraction peaks indicate that this complex crystallized relatively well, forming nanosized crystallites of varying dimensions.

By contrast, PXRD patterns of complexes $[ZrO(MBI)_2]$ and $[ZrO(MtzS)_2]$ were dominated by broad, diffuse humps rather than a sufficient series of resolved Bragg reflections (Figures 3 and 4), indicating a predominantly poorly crystalline (near-amorphous) character. The main hump in the $[ZrO(MBI)_2]$ pattern was centered at $2\theta \approx 30.246°$ with FWHM ≈ 9.726°, giving an apparent D value of about 0.85 nm by the Scherrer equation, together with a secondary broad hump near 53.726° corresponding to an apparent D of about 0.41 nm. Similarly, the main hump in the $[ZrO(MtzS)_2]$ pattern was centered at $2\theta \approx 30.165°$ with FWHM ≈ 10.312°, giving an apparent D of about 0.80 nm, with a secondary hump near 52.619° corresponding to an apparent D of about 0.33 nm (**Table 3**).

Table 3. Crystallite sizes calculated by the Scherrer equation for complexes $[ZRO(MBT)_2]$, $[ZrO(MBI)_2]$ and $[ZrO(MtzS)_2]$.

Complexes	Reflection type	2θ (°)	Intensity (counts)	d (Å)	FWHM (°)	β (rad)	D (nm)
$[ZrO(MBT)_2]$	Sharp	11.725	332.2	7.542	0.278	0.00485	28.77
	Sharp	12.925	219.6	6.844	0.344	0.00601	23.22
	Sharp	22.625	252.0	3.927	0.165	0.00288	49.16
	Sharp	23.125	804.6	3.843	0.181	0.00316	44.76
	Sharp	23.475	527.1	3.787	0.194	0.00339	41.83
	Sharp	24.125	248.6	3.686	0.301	0.00526	26.96
	Sharp	24.875	243.1	3.577	0.305	0.00532	26.69
	Sharp	27.875	920.0	3.198	0.178	0.00311	45.88
	Sharp	28.375	717.8	3.143	0.255	0.00444	32.19
	Sharp	31.975	225.1	2.797	0.220	0.00384	37.56

Complexes	Reflection type	2θ (°)	Intensity (counts)	d (Å)	FWHM (°)	β (rad)	D (nm)
$[ZrO(MBI)_2]$	Main broad hump	30.246	≈146	2.953	9.726	0.16975	0.85*
	Secondary broad hump	53.726	≈84	1.705	21.934	0.38281	0.41*
$[ZrO(MtzS)_2]$	Main broad hump	30.165	≈152	2.960	10.312	0.17998	0.80*
	Secondary broad hump	52.619	≈96	1.738	26.458	0.46178	0.33*

* Values marked with an asterisk are apparent sizes calculated from broad, diffuse humps rather than individual resolved Bragg reflections, and should therefore be regarded as a qualitative indicator of poor crystallinity rather than a precise measure of crystallite size.

The relatively large FWHM values and the diffuse humps observed in the $[ZrO(MBI)_2]$ and $[ZrO(MtzS)_2]$ patterns clearly indicate reduced long-range structural order, consistent with a poorly crystalline or predominantly amorphous character. Although D values can be calculated mathematically for these broad humps, the resulting numbers should not be presented as definitive crystallite sizes, since these features are not well-resolved, individual Bragg reflections, and the contributions of background, instrumental broadening and micro-strain were not deconvoluted from the total peak width. Overall, the PXRD results indicate that complex $[ZrO(MBT)_2]$ possesses a more clearly defined crystalline arrangement than complexes $[ZrO(MBI)_2]$ and $[ZrO(MtzS)_2]$, in which diffuse scattering and poor crystallinity predominate. The Miller indices (hkl) determined experimentally for complex $[ZrO(MBT)_2]$ from the $\sin^2\theta$ values are given in **Table 4**.

Table 4. Experimentally determined Miller indices (hkl) for complex $[ZrO(MBT)_2]$, based on the modified Bragg relationship.

2θ (°)	$\sin^2\theta$	Normalized value	Nearest integer	$h^2+k^2+l^2$ (hkl)
11.725	0.010433	1	3	111
12.925	0.012668	1.214	4	200
22.625	0.038479	3.688	11	311
23.125	0.040175	3.851	12	222
23.475	0.041383	3.967	12	222
24.125	0.043672	4.186	13	320
24.875	0.046386	4.446	13	320
27.875	0.058015	5.561	17	322, 410
28.375	0.060072	5.758	17	322, 410
31.975	0.075860	7.271	22	332

2θ: Bragg angle. Normalized value: the ratio of each $\sin^2\theta$ value to the smallest $\sin^2\theta$ value (first term). Nearest integer: the normalized value multiplied by a suitable common factor and rounded to the nearest whole number to remove fractional remainders. hkl: the corresponding crystallographic Miller indices.

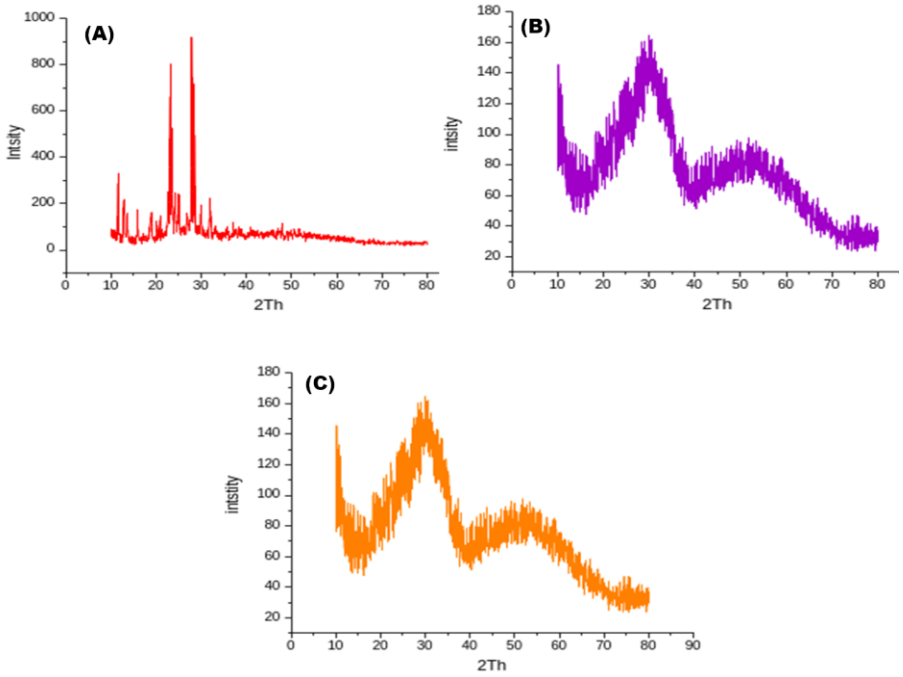


Figure 5. PXRD pattern of (A) [ZrO(MBT)$_2$], (B) [ZrO(MBI)$_2$], (C) [ZrO(MtzS)$_2$].

3.4 SEM images and EDX analysis

Figure 6A shows the SEM picture of the [ZrO(MBT)$_2$] complex (**1**) and the image shows a dense, layered, and somewhat fibrous or plate-like structure with visible cracks and striations. and the particle size annotated measurements range from 15.29 nm to 128.9 nm, indicating a nanoscale material with moderate polydispersity. Whereas the **Figure 6B** displays the SEM image of the [ZrO(MBI)$_2$] complex (**2**) and this image reveals a highly agglomerated, cauliflower-like or granular morphology. The particles are more rounded and clustered compared to complex (**1**), and the particle size range from 56.86 nm to 229.9 nm, showing a broader size distribution and larger agglomerates. The smallest particles (56–79 nm) are visible within the clusters, while the larger values (100–230 nm) likely represent agglomerated assemblies. The SEM Image of the [ZrO(MtSz)$_2$] complex (**3**) showed in **Figure6C** and the image displays a highly agglomerated, cauliflower-like or granular morphology. The particles are spherical to irregular in shape and are densely packed into larger clusters. Visually, this morphology is very similar to that of complex (**2**) [ZrO(MBI)$_2$] (Figure 2), suggesting that the two complexes may have similar crystallization or aggregation behavior. In contrast, complex (**1**) [ZrO(MBT)$_2$] (**Figure 6A**) exhibited a more layered, fibrous, or plate-like structure. Whereas the particle size ranges from 38.21 nm to 203.0 nm. The elemental composition of the ZCO and NiO-ZCO composite, as determined by energy dispersive X-ray analysis (EDX), is shown in **Figure 7A-Z**. It was confirmed that Zn, Co, Ni, and O were present in the composite.

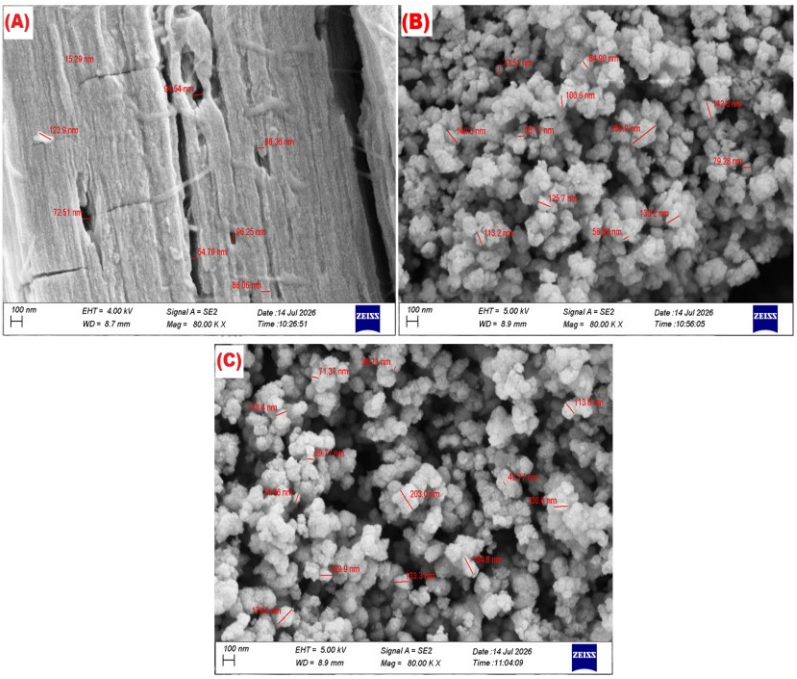


Figure 6. SEM picture of the (A) $[ZrO(MBT)_2]$, (B) $[ZrO(MBI)_2]$, (C) $[ZrO(MtzS)_2]$.

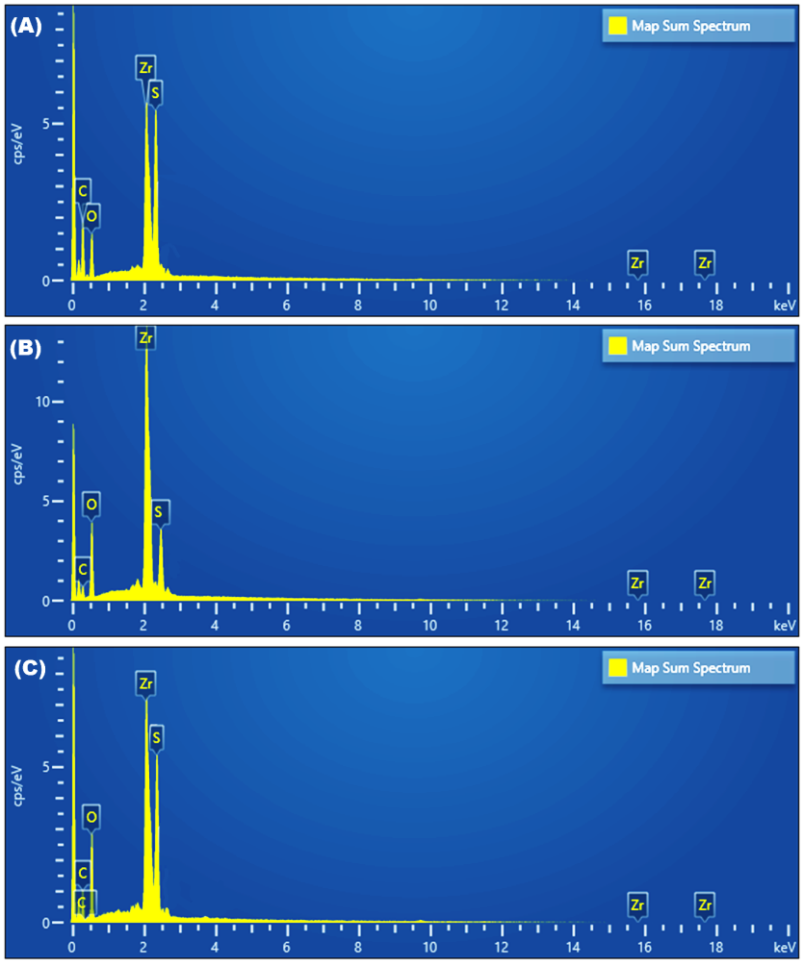


Figure 7. EDX picture of the (A) $[ZrO(MBT)_2]$, (B) $[ZrO(MBI)_2]$, (C) $[ZrO(MtzS)_2]$.

3.5 Biological activity

The biological activity of the free thione ligands {benzo[d]thiazole-2-thiol (HMBT), 1H-benzo[d]imidazole-2-thiol (HMBI), 1-methyl-1H-tetrazole-5-thiol (HMtzS)} and their zirconium (IV) complexes {[ZrO(MBT)$_2$], [ZrO(MBI)$_2$], [ZrO(MtzS)$_2$]} was evaluated against three bacterial strains: ***Staphylococcus aureus*** (Gram-positive), ***Staphylococcus epidermidis*** (Gram-positive), and ***Escherichia coli*** (Gram-negative) (**Table 5** and **Figure 8**). The activity was measured as the diameter of the inhibition zone (DIZ, in mm), with tetracycline used as a standard antibiotic control.

Table 5. Diameter inhibition zone (mm) of free ligands and its complexes

Tested compounds	*staphylococcus aureus*	*Staphylococcus epidermidis*	*Escherichia coli*
HMBT	6	8	7
HMBI	9	10	8
HMtzS	8	11	9
[ZrO(MBT)$_2$]	16	14	13
[ZrO(MBI)$_2$]	19	17	18
[ZrO(MtzS)$_2$]	17	21	14
Tetracycline	23	25	21

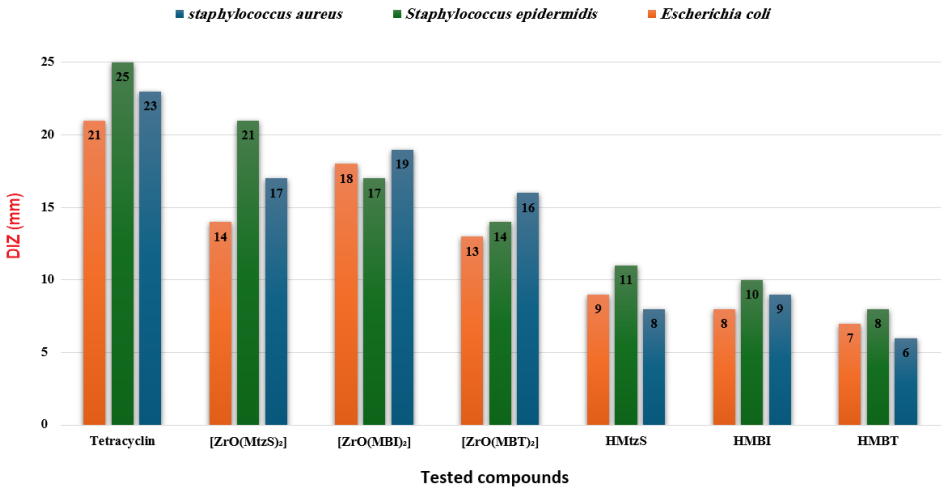


Figure 8: Histogram of the biological activity of the of free ligands and their complexes

All three free ligands (HMBT, HMBI, HMtzS) showed only modest activity against the tested bacterial strains, with inhibition zones ranging from **6–11 mm**. Among them, **HMtzS** was the most active against *S. epidermidis* (11 mm), while **HMBI** showed the highest activity against *S. aureus* (9 mm). *E. coli* was generally the least susceptible to the free ligands.

Upon coordination with zirconium (IV), all three complexes exhibited markedly increased antibacterial activity compared to their respective free ligands. This enhancement is consistent with the well-known phenomenon that metal complexation often increases the lipophilicity and membrane permeability of ligands, facilitating their penetration through the bacterial cell wall.

1. **[ZrO(MBI)$_2$]** showed the most balanced and potent activity against all three strains: *S. aureus* (19 mm), *S. epidermidis* (17 mm), and *E. coli* (18 mm).
2. **[ZrO(MtzS)$_2$]** was particularly effective against *S. epidermidis* (21 mm), the highest among all complexes for this strain.

3. **[ZrO(MBT)$_2$]** displayed moderate activity, with inhibition zones of 16, 14, and 13 mm against *S. aureus*, *S. epidermidis*, and *E. coli*, respectively.

Although the Zr(IV) complexes showed strong antibacterial activity, they did not surpass the standard antibiotic **tetracycline** (23–25 mm). However, the complexes approached tetracycline's efficacy, especially **[ZrO(MBI)$_2$]** and **[ZrO(MtzS)$_2$]**, indicating their potential as promising antibacterial agents.

4. Discussion

The differences may be attributed to variations in the electronic environment, steric bulk, and lipophilicity imparted by the different heterocyclic rings, affecting bacterial membrane penetration and intracellular target interaction. The complexes generally showed slightly higher activity against Gram-positive strains (*S. aureus and S. epidermidis*) compared to Gram-negative *E. coli*. This is typical, as Gram-negative bacteria possess an outer membrane that acts as an additional permeability barrier. However, [ZrO(MBI)$_2$] was equally effective against *E. coli* (18 mm), suggesting that this complex may overcome the outer membrane barrier more effectively.

5. Conclusion

were synthesized and characterized successfully. Spectroscopic and analytical studies indicated that all the ligands coordinate to Zr(IV) in bidentate manner (S,N) through the deprotonated thiolate sulfur and heterocyclic nitrogen to give non-electrolytic complexes. The PXRD analysis revealed a relatively crystalline structure of [ZrO(MBT)$_2$] with an average crystallite size of ~ 35.7 nm, while [ZrO(MBI)$_2$] and [ZrO(MtzS)$_2$] are predominantly amorphous. SEM revealed different morphologies, a layered, fibrous structure for [ZrO(MBT)$_2$] and agglomerated, cauliflower-like granules for the other two complexes, with particle sizes ranging from 38 to 230 nm. EDX analysis confirmed the presence of Zr, S, O, C and N. The antibacterial evaluation showed that all the complexes have significantly increased activity over their free ligands, with [ZrO(MBI)$_2$] being the most balanced and potent against all three strains, and [ZrO(MtzS)$_2$] being the most effective against S. epidermidis. The complexes were not better than tetracycline but near to it, which indicates that they are promising antibacterial agents. The variations in activity are attributed to variations in electronic environment, steric bulk and lipophilicity. This work adds to zirconium-thione coordination chemistry and future work should include single crystal structure determination and mechanistic studies.

REFERENCES

[1] T. E. Macdermott, "The structural chemistry of zirconium compounds," *Coordination Chemistry Reviews*, vol. 11, no. 1, pp. 1–20, 1973.

[2] R. J. H. Clark, D. C. Bradley, and P. Thornton, *The Chemistry of Titanium, Zirconium and Hafnium: Pergamon Texts in Inorganic Chemistry*, vol. 19. Oxford, U.K.: Elsevier, 2018.

[3] D. V. Aleksanyan and V. A. Kozlov, "Pincer complexes with thione sulfur donors," in *The Privileged Pincer-Metal Platform: Coordination Chemistry & Applications*, pp. 209–238. Cham, Switzerland: Springer International Publishing, 2015.

[4] S. Sinha, A. K. Srivastava, C. M. Tripathi, O. P. Pandey, and S. K. Sengupta, "Synthesis, spectroscopic, and antimicrobial studies of binuclear metallocene (M = Ti, Zr, or Hf) derivatives of bis(mercaptoazoles)," *Bioinorganic Chemistry and Applications*, vol. 2007, no. 1, Art. no. 087918, 2007.

[5] E. S. Raper, "Complexes of heterocyclic thione donors," *Coordination Chemistry Reviews*, vol. 61, pp. 115–184, 1985.

[6] P. Cassoux, L. Valade, H. Kobayashi, A. Kobayashi, R. A. Clark, and A. E. Underhill, "Molecular metals and superconductors derived from metal complexes of 1,3-dithiol-2-thione-4,5-dithiolate (dmit)," *Coordination Chemistry Reviews*, vol. 110, no. 1, pp. 115–160, 1991.

[7] R. M. Olk, B. Olk, W. Dietzsch, R. Kirmse, and E. Hoyer, "The chemistry of 1,3-dithiole-2-thione-4,5-dithiolate (dmit)," *Coordination Chemistry Reviews*, vol. 117, pp. 99–131, 1992.

[8] E. S. Raper, "Complexes of heterocyclic thionates. Part 1. Complexes of monodentate and chelating ligands," *Coordination Chemistry Reviews*, vol. 153, pp. 199–255, 1996.

[9] E. S. Raper, "Copper complexes of heterocyclic thioamides and related ligands," *Coordination Chemistry Reviews*, vol. 129, no. 1–2, pp. 91–156, 1994.
[10] E. S. Raper, "Complexes of heterocyclic thionates. Part 2: Complexes of bridging ligands," *Coordination Chemistry Reviews*, vol. 165, pp. 475–567, 1997.
[11] P. D. Akrivos, "Recent studies in the coordination chemistry of heterocyclic thiones and thionates," *Coordination Chemistry Reviews*, vol. 213, no. 1, pp. 181–210, 2001.
[12] A. S. Al-Janabi, M. A. Alheety, A. Y. Osama'a, S. Shaaban, B. Kibar, and E. Cacan, "Anti-cancer and anti-fungal evaluation of novel palladium(II) 1-phenyl-1H-tetrazol-5-thiol complexes," *Inorganic Chemistry Communications*, vol. 121, Art. no. 108193, 2020.
[13] A. S. Al-Janabi, H. M. Jerjes, and M. H. Salah, "Synthesis and characterization of new metal complexes of thione and phosphines ligands," *Tikrit Journal of Pure Science*, vol. 22, no. 9, p. 53, 2017.
[14] A. S. Al-Janabi, "Synthesis, characterization and study of mercury(II) complexes with phosphine and heterocyclic thiones," *Tikrit Journal of Pure Science*, vol. 20, p. 4, 2015.
[15] A. S. Al-Janabi, O. A. A. Al-Samrai, and T. A. Yousef, "New palladium(II) complexes with 1-phenyl-1H-tetrazole-5-thiol and diphosphine: Synthesis, characterization, biological, theoretical calculations and molecular docking studies," *Applied Organometallic Chemistry*, vol. 34, no. 12, Art. no. e5967, 2020.
[16] A. S. Faihan, M. R. Hatshan, A. S. Alqahtani, F. A. Nasr, S. A. Al-Jibori, and A. S. Al-Janabi, "New divalent metal ion complexes with 1,8-diaminonaphthalene-2-thione: Synthesis, spectroscopic, antibacterial and anticancer activity studies," *Journal of Molecular Structure*, vol. 1247, Art. no. 131291, 2022.
[17] K. T. Abdullah, A. S. Al-Janabi, N. J. Hussien, T. A. Yousef, S. Shaaban, M. I. Attia, and O. K. Al Duaij, "Spectroscopic and biological studies of Pd(II) complexes of 5-(p-tolyl)-1,3,4-oxadiazole-2-thiol," *Bulletin of the Chemical Society of Ethiopia*, vol. 39, no. 1, pp. 79–90, 2025.
[18] S. A. Ahmed and A. S. Al-Janabi, "Synthesis, spectroscopic characterization of Co(II), Ni(II) and Cu(II) complexes with 2-mercapto-5-(2,4-dinitrophenyl)-1,3,4-oxadiazole or 2-mercapto-5-((4-(dimethylamino)benzylidene)amino)-1,3,4-thiadiazole ligands," *Oriental Journal of Chemistry*, vol. 34, no. 4, p. 787, 2018.
[19] O. D. Al-Mouqdady, A. S. Al-Janabi, M. R. Hatshan, S. A. Al-Jibori, A. S. Faihan, and C. Wagner, "Synthesis, characterization, antibacterial and anticancer activities of palladium(II) mixed ligand complexes of 2-mercapto-5-methyl-1,3,4-thiadiazole (HmtzS) and phosphines. Crystal structure of $[Pd(mtzS)_2(dppf)]\cdot H_2O\cdot EtOH$," *Journal of Molecular Structure*, vol. 1264, Art. no. 133219, 2022.
[20] A. A. Hameed, A. S. Al-Janabi, S. A. Al-Jibori, M. A. Alheety, and P. K. Singh, "Exploration of novel phenyl mercury tetrazole-thione complexes: Characterization and investigating the impact of diamine ligands on enhanced hydrogen storage," *Energy Storage*, vol. 6, no. 2, Art. no. e598, 2024.
[21] M. R. Dawood, A. S. Al-Janabi, and A. S. Faihan, "Zinc(II) mixed ligand complexes of acesulfame and thiones: Structural characterization and biological activity," *Journal of Biomimetics, Biomaterials and Biomedical Engineering*, vol. 71, pp. 17–32, 2026.
[22] A. S. Al-Janabi, U. A. A. Al-Samra, E. A. Othman, and T. A. Yousef, "Optical properties, structural, and DFT studies of Pd(II) complexes with 1-phenyl-1H-tetrazol-5-thiol, X-ray crystal structure of $[Pd(\kappa1\text{-}S\text{-}ptt)_2(\kappa2\text{-}dppe)]$ complex," *Applied Organometallic Chemistry*, vol. 34, no. 12, Art. no. e5996, 2020.
[23] A. S. Faihan, R. H. AlShammari, M. Ashfaq, S. Muhammad, S. A. Al-Jibori, M. N. Tahir, *et al.*, "Synthesis, spectroscopic, crystallographic, quantum and molecular docking investigations of cis-4,5-diphenylimidazolidine-2-thione," *Journal of Molecular Structure*, vol. 1286, Art. no. 135633, 2023.
[24] S. A. Ahmed, A. S. M. Al-Janabi, and S. A. Ahmed, "Synthesis and characterization of mercury(II) mixed ligands complexes derived from 5-(4-pyridyl)-1,3,4-oxadiazole-2-thione with tertiary phosphines ligands," *Kirkuk Journal of Science*, vol. 12, no. 2, pp. 9–25, 2017.
[25] A. S. Al-Janabi, O. D. Al-Mouqdady, M. E. Al-Doori, H. Ferjani, O. K. Al Duaij, Z. A. Alothman, and T. A. Yousef, "Synthesis and characterization of new HgS nanoparticles prepared by Hg(II)-triazole-3-thiol as precursor," *Journal of Saudi Chemical Society*, vol. 26, no. 4, pp. 1–10, 2022.
[26] A. A. Hameed, A. S. Al-Janabi, A. M. Saleh, S. Shaaban, and M. Alheety, "Spectroscopic, biological activity, molecular docking and hydrogen storage studies of tetrazole-thione complexes," *Journal of Molecular Structure*, vol. 1312, Art. no. 138672, 2024.
[27] A. Y. Osama'a, A. S. Al-Janabi, and E. A. Othman, "Mixed ligand complexes of Hg-tetrazole-thiolate with phosphine: Synthesis and spectroscopic studies," *Tikrit Journal of Pure Science*, vol. 24, no. 5, pp. 10–17, 2019.

[28] A. Y. Osama'a, O. R. Al Samarrai, T. A. Yousef, M. M. Abou-Krisha, M. H. Alhalafi, and A. S. Al-Janabi, "Synthesis, spectroscopic, DFT, anticancer evaluation and enzyme inhibition studies of platinum(II) complexes with 1-methyl-1H-1,2,3,4-tetrazole-5-thiol and phosphine ligands: Crystal structure of [Pt(mtzt)$_2$(dppe)]," *Chemical Physics Impact*, vol. 8, Art. no. 100581, 2024.
[29] A. S. Al-Janabi, B. H. Abdullah, and S. A. Al-Jibori, "Synthesis, crystal structure and spectral studies of mercury(II) complexes containing the mixed ligands benz-1,3-imidazoline-2-thione, benz-1,3-oxazoline-2-thione, benz-1,3-thiazoline-2-thione, and diphosphine," *Oriental Journal of Chemistry*, vol. 25, no. 2, p. 277, 2009.
[30] O. D. Al-Mouqdady, M. R. Hatshan, A. S. Faihan, M. A. Alheety, and A. S. Al-Janabi, "Mercury(II)-complex with 5-methyl-1,3,4-thiadiazole-2-thiol: Kinetic studies of hydrogen storage," *International Journal of Hydrogen Energy*, vol. 47, no. 59, pp. 24852–24860, 2022.
[31] A. S. Al-Janabi, "Synthesis, characterization and study of mercury(II) complexes with phosphine and heterocyclic thiones," *Tikrit Journal of Pure Science*, vol. 20, no. 4, pp. 1–7, 2015.
[32] A. S. Al-Janabi, O. A. A. Al-Samrai, and T. A. Yousef, "New palladium(II) complexes with 1-phenyl-1H-tetrazole-5-thiol and diphosphine: Synthesis, characterization, biological, theoretical calculations and molecular docking studies," *Applied Organometallic Chemistry*, vol. 34, no. 12, Art. no. e5967, 2020.
[33] A. S. Faihan, M. R. Hatshan, A. S. Alqahtani, F. A. Nasr, S. A. Al-Jibori, and A. S. Al-Janabi, "New divalent metal ion complexes with 1,8-diaminonaphthalene-2-thione: Synthesis, spectroscopic, antibacterial and anticancer activity studies," *Journal of Molecular Structure*, vol. 1247, Art. no. 131291, 2022.
[34] K. T. Abdullah, A. S. Al-Janabi, N. J. Hussien, T. A. Yousef, S. Shaaban, M. I. Attia, and O. K. Al Duaij, "Spectroscopic and biological studies of Pd(II) complexes of 5-(p-tolyl)-1,3,4-oxadiazole-2-thiol," *Bulletin of the Chemical Society of Ethiopia*, vol. 39, no. 1, pp. 79–90, 2025.
[35] S. A. Ahmed and A. S. Al-Janabi, "Synthesis, spectroscopic characterization of Co(II), Ni(II) and Cu(II) complexes with 2-mercapto-5-(2,4-dinitrophenyl)-1,3,4-oxadiazole or 2-mercapto-5-((4-(dimethylamino)benzylidene)amino)-1,3,4-thiadiazole ligands," *Oriental Journal of Chemistry*, vol. 34, no. 4, pp. 787–794, 2018.
[36] O. D. Al-Mouqdady, A. S. Al-Janabi, M. R. Hatshan, S. A. Al-Jibori, A. S. Faihan, and C. Wagner, "Synthesis, characterization, antibacterial and anticancer activities of palladium(II) mixed ligand complexes of 2-mercapto-5-methyl-1,3,4-thiadiazole (HmtzS) and phosphines. Crystal structure of [Pd(mtzS)$_2$(dppf)]·H$_2$O·EtOH," *Journal of Molecular Structure*, vol. 1264, Art. no. 133219, 2022.
[37] A. A. Hameed, A. S. Al-Janabi, S. A. Al-Jibori, M. A. Alheety, and P. K. Singh, "Exploration of novel phenyl mercury tetrazole-thione complexes: Characterization and investigating the impact of diamine ligands on enhanced hydrogen storage," *Energy Storage*, vol. 6, no. 2, Art. no. e598, 2024.
[38] M. R. Dawood, A. S. Al-Janabi, and A. S. Faihan, "Zinc(II) mixed ligand complexes of acesulfame and thiones: Structural characterization and biological activity," *Journal of Biomimetics, Biomaterials and Biomedical Engineering*, vol. 71, pp. 17–32, 2026.
[39] A. S. Al-Janabi, U. A. A. Al-Samra, E. A. Othman, and T. A. Yousef, "Optical properties, structural, and DFT studies of Pd(II) complexes with 1-phenyl-1H-tetrazol-5-thiol, X-ray crystal structure of [Pd(κ1-S-ptt)$_2$(κ2-dppe)] complex," *Applied Organometallic Chemistry*, vol. 34, no. 12, Art. no. e5996, 2020.
[40] A. S. Faihan, R. H. AlShammari, M. Ashfaq, S. Muhammad, S. A. Al-Jibori, M. N. Tahir, *et al.*, "Synthesis, spectroscopic, crystallographic, quantum and molecular docking investigations of cis-4,5-diphenylimidazolidine-2-thione," *Journal of Molecular Structure*, vol. 1286, Art. no. 135633, 2023.
[41] S. A. Ahmed, A. S. M. Al-Janabi, and S. A. Ahmed, "Synthesis and characterization of mercury(II) mixed ligands complexes derived from 5-(4-pyridyl)-1,3,4-oxadiazole-2-thione with tertiary phosphines ligands," *Kirkuk Journal of Science*, vol. 12, no. 2, pp. 9–25, 2017.
[42] A. S. Al-Janabi, O. D. Al-Mouqdady, M. E. Al-Doori, H. Ferjani, O. K. Al Duaij, Z. A. Alothman, and T. A. Yousef, "Synthesis and characterization of new HgS nanoparticles prepared by Hg(II)-triazole-3-thiol as precursor," *Journal of Saudi Chemical Society*, vol. 26, no. 4, pp. 1–10, 2022.
[43] A. A. Hameed, A. S. Al-Janabi, A. M. Saleh, S. Shaaban, and M. Alheety, "Spectroscopic, biological activity, molecular docking and hydrogen storage studies of tetrazole-thione complexes," *Journal of Molecular Structure*, vol. 1312, Art. no. 138672, 2024.
[44] A. Y. Osama'a, A. S. Al-Janabi, and E. A. Othman, "Mixed ligand complexes of Hg-tetrazole-thiolate with phosphine: Synthesis and spectroscopic studies," *Tikrit Journal of Pure Science*, vol. 24, no. 5, pp. 10–17, 2019.